ICARUS **119,** 90–111 (1996)
ARTICLE NO. 0004

Ultraviolet Spectroscopy of the SL9 Impact Sites

I. The 175–230 nm Region

ROGER V. YELLE

NASA Ames Research Center, Moffett Field, California 94035
E-mail: yelle@vega.lpl.arizona.edu

AND

MELISSA A. MCGRATH

Space Telescope Science Institute, Baltimore, Maryland 21218

Received March 2, 1995; revised August 23, 1995

We present a comprehensive analysis of spectra in the 175–230 nm wavelength region obtained by the Faint Object Spectrograph of the Hubble Space Telescope (HST) to determine the abundance of molecular species in the vicinity of the G and L impact sites. Data were obtained on July 18, roughly 3 hr after the G impact, on August 9, and on August 23. All spectra clearly show signatures of aerosols and gaseous CS_2 and NH_3. The spectra obtained on July 18 also show the spectral signature of H_2S. To determine the abundance of gases and aerosols we compare the observations with calculations based on the scattering properties of three-layer models for the atmosphere. We are able to fit the aerosol-dominated portions of the spectra with aerosol distributions similar to those derived from HST imaging observations by West *et al.* (*Science,* 267, 1296–1301, 1995). On all three dates we find that CS_2 resides at lower pressures than H_2S, NH_3, and the bulk of the aerosols. The CS_2 column abundance is approximately 10^{-7} g-cm^{-2} on July 18, a factor of 2–3 less on August 9, and another factor of 2 less on August 23. NH_3 is confined to pressures greater than 5 mbar with a mole fraction of 1×10^{-7} on July 18 and August 9, decreasing to 3×10^{-8} on August 23. H_2S is also confined to pressures greater than 5 mbar with a mole fraction of 5×10^{-8} on July 18. These mole fractions depend upon assumptions about the aerosol distribution and are derived from models with an aerosol column density of 2×10^{9} cm^{-2}. Using different aerosol models, it is possible to obtain adequate fits to the spectra with mole fractions of H_2S and NH_3 that are 2.5 and 7.5 times smaller. The spectra show no evidence for SO_2 absorption and we derive an upper limit of 10^{-7} g-cm^{-2} for the July 18 spectrum, assuming that SO_2 has the same altitude distribution as CS_2. Using the same assumptions we derive upper limits of 10^{-6} and 3×10^{-8} for OCS and SO. There is no compelling evidence for either H_2O or C_2H_2 but both can be tolerated with mole fractions of 1×10^{-7} and 3×10^{-7}, respectively. The altitude distributions of CS_2, H_2S, and NH_3 suggest that CS_2 was created by chemistry in the plume but that H_2S and NH_3 were injected into the stratosphere from below by upwelling over spatial scales of thousands of kilometers associated with the impact. The presence of H_2S on July 18 suggests that the G fragment penetrated at least as deep as the NH_4–SH clouds.

I. INTRODUCTION

For a period of about 1 week beginning on July 16, 1994, Jupiter was bombarded by the fragments of comet p/Shoemaker–Levy 9 (SL9). The collision between the cometary fragments and jovian atmosphere produced a spectacular array of observable phenomena including plumes, waves, infrared brightening of the atmosphere, and widespread debris patterns around the impact sites (Clarke *et al.* 1995, Hammel *et al.* 1995, Noll *et al.* 1995, Orton *et al.* 1995, West *et al.* 1995). The chemical composition of the atmosphere was altered by the impacts (Lellouch *et al.* 1995, Marten *et al.* 1995, Maillard *et al.* 1995; Noll *et al.* 1995, Orton *et al.* 1995, Roos-Serote *et al.* 1995). Spectroscopic observations from ground- and space-based observatories have led to the detection of numerous species newly visible in the jovian atmosphere and have revealed changes in the abundance of the usually visible constituents. It is these chemical changes to the jovian atmosphere that are the subject of the present paper.

The changes in the chemical composition of the atmosphere caused by the collision provide important constraints on the nature of the impacts. The ensemble of newly discovered species reflects the composition of the impactor and of the jovian atmosphere and the physical

0019-1035/96 $12.00

conditions in the explosion. Moreover, the altitude distribution of the chemical constituents and their relationship to aerosols in the atmosphere should provide insight into the dynamics of the impact process. Drawing definitive conclusions on these subjects will require correlative study of diverse observations and comparison with the models being developed to describe the impact. Here, we begin this process by analyzing a subset of the Hubble Space Telescope (HST) spectroscopic observations to determine the abundance and altitude distribution of CS_2, H_2S, and NH_3 and to place limits on the abundance of some other constituents.

One interesting result of these chemical investigations is the discovery of the sulfur-bearing molecules, S_2, CS_2, H_2S, CS, and OCS in the jovian atmosphere (Noll *et al.* 1995, Lellouch *et al.* 1995). Although it has been hypothesized that sulfur compounds are responsible for some of the colors seen on Jupiter, sulfur-bearing molecules have not previously been detected on any of the outer planets. Because sulfur is a common element in the sun and in meteorites (Anders and Grevese 1989), it is believed to have been present in the solar nebula and should have been incorporated in Jupiter as it formed. According to thermochemical considerations, essentially all the sulfur in Jupiter's deep atmosphere should be in the form of H_2S, which, prior to SL9, had not been detected (cf. Fegley and Lodders 1994, and references therein). Lewis (1969) was the first to argue that non-detection is to be expected because H_2S should condense out at relatively deep, unobservable levels in the atmosphere, along with NH_3, forming NH_4–SH clouds. Current knowledge of the pressure–temperature profile in the jovian atmosphere places the base of the NH_4–SH clouds near a pressure of 2 bars (Larson *et al.* 1984).

In addition to sulfur species, enhanced NH_3 in the jovian atmosphere has been detected in both UV and IR spectra (Noll *et al.* 1995, Orton *et al.* 1995, Griffith *et al.*, in preparation). NH_3 is believed to be the primary constituent of the visible clouds in the jovian atmosphere; it is also visible in the UV as a trace gas just above the NH_3 cloud deck even in the unperturbed jovian atmosphere (cf. West *et al.* 1986). We find that the impacts inject NH_3 into the jovian stratosphere to pressures as low as a few millibars. The H_2S observed by HST appears to reside at similar pressures. This fact, and other considerations, suggest that these species are jovian in origin (i.e., they were not synthesized in the plume) and have been transported from the deep atmosphere to the stratosphere by processes associated with the impacts. If this deduction is correct, it yields important insight into the energy partitioning in the explosion.

Although many oxygen-bearing molecules absorb in the UV spectral range, none have been definitively detected in our observations. SO_2, in particular, is absent. The lack of SO_2 is important because it should be a primary product of thermochemistry in a roughly solar composition gas heated to high temperatures (Zahnle *et al.* 1995). This in turn implies that the gas involved in the chemistry was lacking in oxygen and therefore was derived primarily from jovian air in the region between the NH_4–SH cloud and H_2O cloud. Models for the explosion of the bolide imply that impactors with diameters in the range 0.5–1.0 m will penetrate to this depth (MacLow and Zahnle 1994).

This paper concentrates exclusively on observations with the Hubble Space Telescope Faint Object Spectrograph (FOS) with the G190H grating, which covers the 175–230 nm spectral region. Preliminary results from these spectra have been published by Noll *et al.* (1995). Here, we fully document the data reduction and present a more comprehensive analysis of the spectra. The results presented here supersede those in Noll *et al.* (1995). Subsequent papers in the series will present reduction and analysis of the G270H grating spectra, which covers the 230–320 nm spectral region and displays prominent S_2 absorption features, and of limb observations, which reveal emission features from numerous species including CS, Si, Mg, Mg^+, and Fe^+ (Noll *et al.* 1995).

II. OBSERVATIONS AND DATA REDUCTION

We analyze in detail three sets of observations obtained with the HST FOS on July 18, August 9, and August 23, 1994. In addition, we make use of a spectrum with an identical instrument setup and nearly identical pointing obtained in July 14, 1994, before the impacts began. Detailed information about the observations has been presented in Noll *et al.* (1995; see their Table 1), and additional information is given in Table I. All observations use the 0.86″ aperture with grating G190H, covering the wavelength region 157–231 nm at ~0.4 nm resolution. At the short-wavelength end of the range covered, the detector has low sensitivity, resulting in a low signal-to-noise ratio (S/N). Since the grating and detector are not solar blind, the data also suffer from contamination by longer wavelength, internal grating scattered light in this region. This is illustrated by the spectrum from the July 18 observation shown in Fig. 1a, where the combination of low detector sensitivity and scattered light contamination cause a sharp upturn in the spectrum and albedo shortward of ~170 nm which may be due to an incorrect scattered light correction rather than a real change in the reflectivity of Jupiter. We therefore limit analysis in this paper to wavelengths above 175 nm. A detailed comparison between the FOS data and Goddard High Resolution Spectrograph observations (which do not suffer significantly from grating scattered light contamination) of the G impact site taken on July 21, 1994 may eventually make a quantitative correction for the grating scattered light in the FOS data possible and allow more detailed analysis of the data below 175 nm.

TABLE I
Viewing Geometry

Date	Time (UT)	Lat, Lon (system III)	Emission angle	Incidence angle	Azimuthal angle
July 14	18:41	−48.7, 18.0	73	66	170.7
July 18	11:06	−49.2, 18.1	54	50	167.7
July 21	16:13	−49.7, 28.8	73	80	170.7
August 9	10:42	−49.5, 28.7	79	72	170.7
August 23	01:18	−47.2, 10.4	67	61	170.3

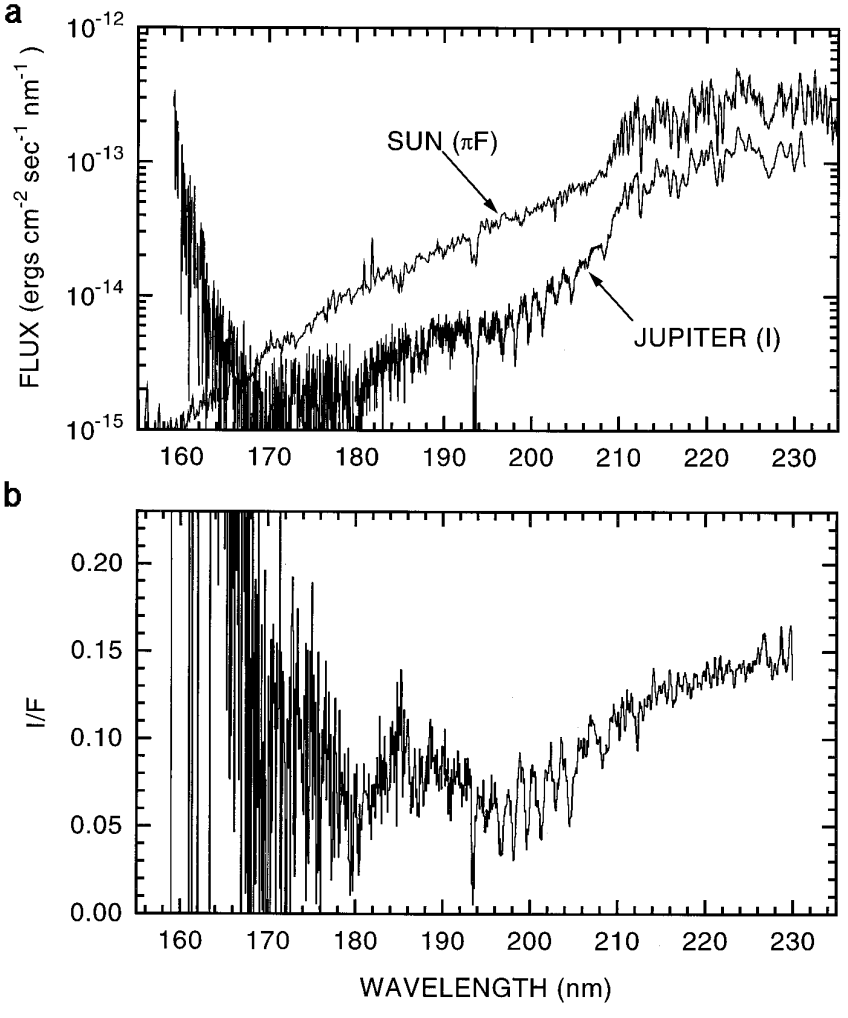

FIG. 1. (a) The bottom trace shows the UV flux from Jupiter within the FOS aperture and the top trace the solar flux, arbitrarily scaled, for comparison with the planetary spectrum. Most of the features longward of 210 nm in the planetary spectrum are simply reflections of solar features but the strong absorptions from 180 to 210 nm are clearly visible in the data, even in this relatively unprocessed form. (b) The reflectivity of the jovian atmosphere (I/F) obtained by dividing flux from the planet by the scaled solar flux. Note the degradation in data quality at short wavelengths. The reasons for this are discussed in the text. The FOS spectra shown here were obtained on July 18, 1994.

The standard data acquisition strategy for FOS observations assumes that the target is a point source. To meet the Nyquist sampling criteria each of the 516 diodes is sampled 4 times in a ''quarter-stepping'' strategy. Hence a typical FOS spectrum contains 2064 data points. An extended source such as Jupiter subtends 3 diodes on the detector instead of the single diode subtended by a point source. As a consequence, spectra from an extended source are significantly oversampled. Therefore, in our data reduction we have binned the data by a factor of 2 to produce a spectrum with 1032 data points. This is still slightly oversampled and we subsequently smooth the data with a 3-point boxcar function for analysis and presentation. The data shown in Fig. 1 have not been smoothed, to illustrate the degradation of reliability below 175 nm.

To calculate the reflectivity of Jupiter we first convert the fluxes measured by the FOS to intensities by dividing by the solid angle of the 0.86″ aperture. We then divide the jovian intensities by the solar flux, corrected to the distance of Jupiter to produce and *I/F* spectrum. The SUSIM solar spectrum (Van Hoosier *et al.* 1988) is used to represent the solar flux, after it is smoothed and resampled to match the resolution and sampling rate of the FOS observations. It is also necessary to slightly adjust the wavelength scale of the SUSIM spectrum to precisely match the locations of prominent solar emission lines.

Even if the process described here is done with great care the resulting spectrum typically contains a significant amount of high-frequency noise caused by slight differences in lineshapes or misalignments between the FOS spectra and the solar spectrum. To eliminate these spurious noise features we use the following technique. We divide each post-impact observation with the pre-impact observation on July 14. This eliminates the high-frequency noise mentioned above because the post-impact and pre-impact observations were made with the same instrument operated under very similar conditions. We then create an *I/F* spectrum for the July 14 observations as described above, smooth it using a very low-frequency median filter to generate a low-resolution albedo that eliminates any spectral features. The ratio of post-impact to pre-impact spectra is then multiplied by the smoothed July 14 albedo to create the *I/F* for each post-impact set of FOS observations in Table I. This procedure preserves the integrity of the data but removes spurious noise. Comparison of spectra produced with this technique to those produced by simple division of the FOS observations by the solar spectrum reveals that a great deal of noise is removed and no artifacts are introduced into the spectrum. The final *I/F* spectra are shown, along with model fits, in the subsequent sections.

The FOS spectra on July 18 and August 9 were targeted for the center of the G impact site. On August 23 the FOS spectra were targeted for the L impact complex, which is roughly 10° eastward of the G impact site; however, by this time the impact debris, as seen in the visible images, had spread considerably and the G and L complexes had effectively merged (Hammel *et al.* 1995).

III. RADIATIVE TRANSFER MODELS

To derive molecular abundances from the FOS observations we calculate the intensity of reflected sunlight from Jupiter's atmosphere with models for the radiative transfer of UV light based on known and assumed properties for the gaseous constituents and aerosols. The calculations employ a standard doubling-adding technique, similar to many that have been extensively described in the literature (cf. Hansen and Travis 1971). The code used in the calculations is very general and is able to model scattering from complex phase functions and highly structured absorption cross sections. This capability is critical to the analysis because the SL9 impact sites contain both aerosols, with sharply peaked scattering phase functions, and molecular species that absorb solar radiation in bands with spectral features on scales smaller than the FOS resolution. The calculations neglect the effects of polarization because data on the polarization of UV light from the impact sites is unavailable and because it should have a negligible effect on the modeling of gaseous absorption signatures. We assume that scattering is monochromatic and that photons shifted in frequency by vibrational Raman scattering are lost to the atmosphere. This approximation is permissible because the solar flux is a rapidly increasing function of wavelength in the UV and the intensity of photons which have been Raman shifted from shorter wavelengths is negligible compared with the intensity of photons which have been Rayleigh scattered or scattered by aerosols at longer wavelengths. We neglect the small wavelength shifts caused by rotational Raman scattering. We note that because of the increased aerosol content of the atmosphere, Raman scattering from the SL9 impact sites is less important than for the undisturbed jovian atmosphere.

III.1. Aerosols

The gaseous constituents injected into the upper atmosphere by the impactors are seen primarily as spectral absorption features superimposed on a slowly varying continuum. The continuum level is due to a combination of scattering by aerosols and Rayleigh scattering by H_2. The first step in the analysis, therefore, is to model the aerosol and H_2 Rayleigh scattering. We do this with simple models for the atmosphere with the aerosols confined to a single homogeneous layer. The models are based partly on our own analysis and partly on results presented by West *et al.* (1995). We use the Rayleigh scattering cross sections for H_2 in Ford and Browne (1973). We assume that the aerosols can be modeled as homogeneous dielectric

TABLE II
Aerosol Models[a]

Model	Size (μm)	Imaginary index of refraction	Column density (cm^{-2})
I	0.25	0.03	2×10^9
II	0.33	0.02	2×10^9
III	0.13	0.04	2×10^9
IV	0.25	0.04	5×10^8
V	0.29	0.03	5×10^8
VI	0.25	0.028	1×10^9

[a] All models have aerosols distributed uniformly from 0 to 100 mbar except for VI which has the aerosols confined above 5 mbar. The real part of the index of refraction is taken as 1.6. A log–normal size distribution is used with a variance of $b = 0.05$.

spheres and use Mie theory to calculate their absorption and scattering properties.

To determine the aerosol distribution we assume that the 230-nm spectral region is free of gaseous absorption. On both August 9 and 23 the reflectivity of the atmosphere is flat from 220 to 230 nm, implying that aerosols rather than gases, which exhibit more spectral structure, are responsible for the absorption. The July 18 spectrum has a positive slope in the 220–230 nm region. We argue below that this is caused by H_2S absorption. If this is correct then our models predict that the effects of H_2S are absent by 230 nm, at which point the scattering properties of the atmosphere are again dominated by aerosols and H_2. We therefore adjust the aerosol distribution to reproduce the observed reflectivity at 230 nm, then add gaseous absorbers to account for the absorption at shorter wavelengths.

At 230 nm a pure Rayleigh-Raman scattering H_2 atmosphere has a reflectivity of $I/F \approx 0.5$, whereas the observed reflectivity is in the range 0.10–0.15. We conclude that the scattering properties of the atmosphere are dominated by aerosols. Unfortunately, this means that it is difficult to determine the abundance of gaseous absorber relative to H_2 and that uncertainties in the aerosol abundance will be reflected in the derived gaseous abundances. These uncertainties will be discussed in detail.

The properties of the aerosols in the vicinity of the G impact site have been studied by West *et al.* (1995) through analysis of HST imaging data in a variety of filters from the UV to near IR. We find that the aerosol distribution determined from the imaging data also provides a good fit to our spectra. Specifically, we assume that the aerosols have an imaginary index of $k = 0.03$ and a real index of refraction of $n = 1.6$. We use a log–normal distribution to describe their sizes, with a mean radius of $a = 0.25$ μm, and a variance of $b = 0.05$. An aerosol column density of $N = 2 \times 10^9$ cm^{-2}, distributed uniformly above 100 mbar, implies a reflectivity of $I/F = 0.15$, which agrees with the observations of the G impact site on July 18. Although this baseline model, derived from the imaging data, provides a good fit to our spectra, it would be unwise to ascribe too much precision to the particle size, imaginary index, and number density of the aerosols, especially considering the presence of large spatial gradients in the appearance of the atmosphere (Hammel *et al.* 1995, West *et al.* 1995) and the pointing uncertainties in the spectroscopy observations (Noll *et al.* 1995). We therefore investigate the consequences of varying the aerosol properties by examining a number of different aerosol models. We find that we cannot vary the aerosol properties very much from the baseline values and still fit the observations; nevertheless, the uncertainties in the aerosol model do imply significant uncertainties in the derived gaseous abundances. In all cases the real index of refraction is kept at 1.6 and the variance of the log–normal size distribution at 0.05.

Table II lists the parameters for six aerosol models and Fig. 2 shows the spectrum calculated for each, for the geometry of the July 18 observations. The models show that a range of spectral variations are possible within the 175- to 230-nm bandpass. Clearly, the abundances inferred for the gaseous absorbers will depend upon the choice of aerosol model. The spectral variations can be understood in terms of the scattering properties of the aerosols. Figure 3 shows the single scattering albedo ($\tilde{\omega}(\lambda)$) and extinction efficiency (Q_{ex}) (i.e., the ratio of extinction cross section to geometrical cross section) as a function of wavelength for several different values of particle size and imaginary index. For 0.25-μm diameter aerosols, $\tilde{\omega}(\lambda)$ is flat and, as long as the abundance is large, the reflectivity of the atmosphere will also be flat, as shown in model I. If the abundance is smaller and the aerosols are slightly darker, there will be a strong upturn in reflectivity toward shorter wavelengths, as shown in model IV. This occurs because Rayleigh scattering from H_2 makes an important contribution at short wavelengths. A similar effect occurs if the aerosols are small (model III) because $Q_{ex}(\lambda)$ is a strongly increasing function of wavelength, implying that Rayleigh scattering from H_2 is relatively more important at short wavelengths. The opposite effect occurs in models II and VI. For these models the extinction cross section of the aerosols decreases with increasing wavelength, implying that Rayleigh scattering is less important at short wavelengths and the curve of reflectivity versus wavelength has a positive slope.

The aerosol models used here are necessarily oversimplified. Given the limited number of spectra and emission angle coverage available, more complicated models are not warranted. For example, it is likely that k varies with wavelength and that the altitude distribution is far more complicated than we have assumed. We can hope that by examining results from several models the uncertainties introduced by these simplifications are adequately addressed.

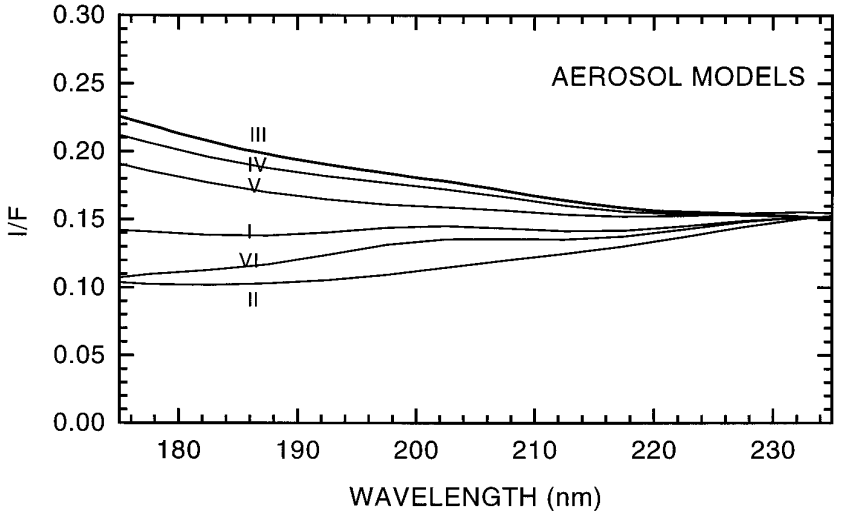

FIG. 2. The variation of reflectivity (I/F) with wavelength for the aerosols models listed in Table II.

It is worth emphasizing that the properties of the aerosols at the G impact site are not all that different from the aerosols usually present in the jovian stratosphere. Tomakso *et al.* (1986) derive a mean particle size of $a = 0.2$ μm and an imaginary index of refraction of $k = 0.052$ at 221 nm for the equatorial atmosphere, which should be compared with the values $a = 0.25$ μm and $k = 0.03$ used here. The aerosols have a dramatic effect on the appearance of the atmosphere because their number has increased as a result of the impact, not because they are significantly darker or have a different size than ambient jovian aerosols. The apparent magnitude of the perturbations is partly fortuitous: the undisturbed jovian atmosphere is characterized by aerosol optical depths on the order of tenths whereas the optical depth after the impact is on the order of several; thus, the change in optical depth is in a regime (i.e., near an optical depth of unity) where it has the maximum effect on the reflectivity of the atmosphere.

III.2. Gaseous Absorbers

To keep our problem tractable we limit our consideration to molecular species such as NH_3 and CS_2 whose effects in the spectrum are obvious, other stable sulfur-bearing molecules such as H_2S, SO, SO_2, and OCS whose presence in the atmosphere might be expected based on the detection of S_2 and CS_2, and other absorbers, including H_2O and C_2H_2, that reside in the atmosphere even when Jupiter is not being bombarded with comet fragments. Figure 4 shows the absorption cross sections for the molecules considered in our analysis. We are able to adequately fit the spectrum at wavelengths longward of 185 nm with models that include only CS_2, H_2S, and NH_3. We will present these models, discuss their uncertainties, then use the best fitting models to place upper limits on other constituents. Initially we will concentrate on the region from 185 to 230 nm. There is apparent absorption at shorter wavelengths but, as discussed earlier, the reflectivity at short wavelengths is not as well determined as that at long wavelengths. We first discuss spectra from July 18 in some detail followed by a briefer summary of model results for the other data sets.

The primary absorbers: CS_2, H_2S, and NH_3. To illustrate the nature of the atmospheric perturbations we show in Fig. 5 a comparison of the July 18 spectrum with one obtained under similar conditions on July 14. Also shown is model fit to the July 14 spectrum. The model atmosphere contains only aerosols and C_2H_2. We assume that the aerosols are uniformly distributed above 100 mbar with a log–normal size distribution having $a = 0.25$ μm, $b = 0.05$, $n = 1.6$, and $k = 0.03$. Under these assumptions we require an aerosol column density of 1×10^8 cm^{-2} to fit the spectrum. [This aerosol abundance is a factor of 20 smaller than that derived for the July 18 post-impact spectrum and is comparable to the aerosol abundance in the undisturbed jovian equatorial regions determined by Tomasko *et al.* (1986).] The C_2H_2 mole fraction in this model is 1×10^{-7}. It is noteworthy that no effects due to NH_3 absorption are evident in the July 14 data. The lack of visibility of NH_3 is due to its depth in the atmosphere coupled with the relatively large solar incidence and emission angles at the impact latitude.

Figure 6 shows the absorption signatures of CS_2, H_2S, and NH_3, along with the July 18 spectrum. The correlation between the observed spectral bands and those of CS_2 is excellent, leaving no doubt about its identification. Although the UV absorption properties of CS_2 have been extensively studied in the laboratory (Xu and Joens 1993, Wu and Judge 1981, Chen and Wu 1995), this is the first

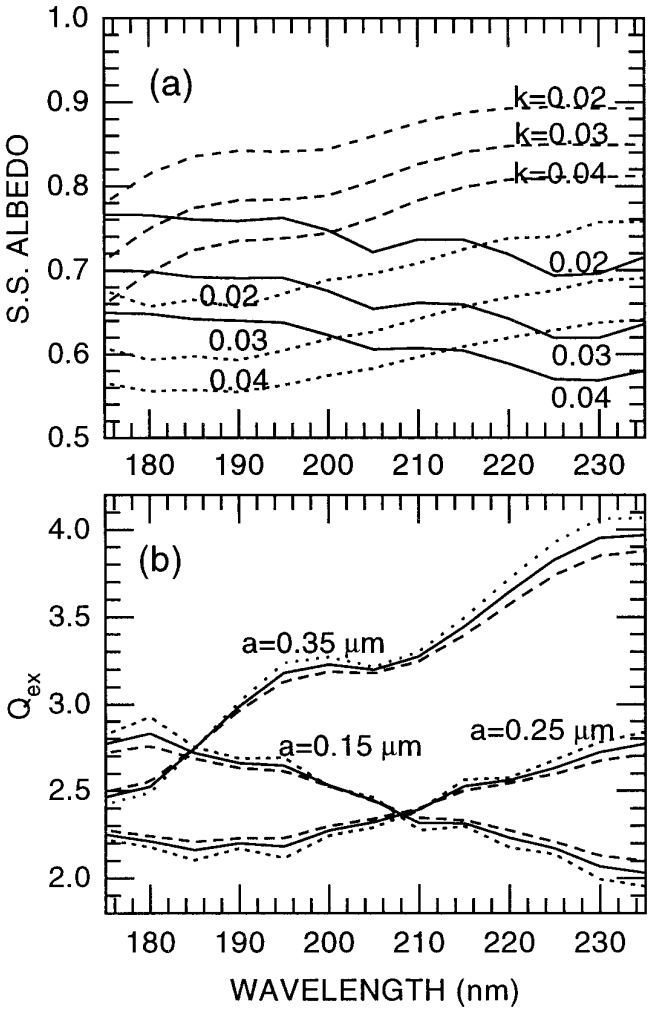

FIG. 3. (a) The single scattering albedo calculated from Mie theory for aerosols with several different sizes and imaginary indices of refraction. The solid curves are calculated with $a = 0.25$ μm, the dotted curves with $a = 0.15$ μm, and the dashed curves with $a = 0.35$ μm. The values of k are indicated on the figure. (b) The extinction coefficient (ratio of extinction cross section to geometrical cross section) calculated from Mie theory for several values of particle size and imaginary index of refraction. The solid curves are calculated with $k = 0.03$, the dotted curves with $k = 0.02$, and the dashed curves with $k = 0.04$. The particle sizes are indicated on the figure.

detection of these features in a planetary atmosphere. The CS_2 cross sections used here were measured at a temperature of 383 K (Chen and Wu 1995).

NH_3 also has features throughout the 185–220 nm region and its effects can be seen in the July 18 spectrum at 213 and 216 nm and, with less confidence, at 186 nm. The visibility of the features implies that NH_3 has been transported by the impact to unusually high levels in the atmosphere. Of course, the deep jovian atmosphere contains significant quantities of NH_3; however, near the tropopause (roughly 100 mbar) NH_3 vapor is destroyed by condensation and photolysis (cf. West *et al.* 1986). Under typical conditions the abundance of NH_3 above 100 mbar is so small that it is undetectable (Wagener *et al.* 1985). Weak absorption features, due to NH_3 in the troposphere are seen with observations made at the disc center (Wagener *et al.* 1985): at a latitude of 45° even these features vanish. Thus, the NH_3 seen in the July 18 spectrum is a consequence of the impact.

Many of the NH_3 features in the 185–220 nm region are nearly coincident with the CS_2 absorption bands. At 194, 197, and 199 nm, however, NH_3 absorbs strongly and CS_2 weakly and it should be possible to see the effects of NH_3 absorption. Surprisingly, all the observed spectra show a maximum in *I/F* at this wavelength. This characteristic of the spectra is extremely important and is discussed in detail below. The NH_3 absorption in the UV is continuous and has a very weak temperature dependence. The cross sections used here were measured at room temperature (Chen *et al.* 1994).

H_2S is the most difficult of the species to constrain because it has a relatively featureless continuum absorption spectrum. Nevertheless, the gradual decrease in *I/F* with decreasing wavelength from 230 to 210 nm in the July 18 spectrum is consistent with H_2S absorption and argues strongly for its presence, especially considering that, as shown later, both the August 9 and August 23 spectra are flat in this region. While it is possible that the decrease in *I/F* from 230 to 210 nm in the July 18 spectrum is due to a variation in the aerosol imaginary index of refraction, we consider this possibility unlikely for reasons discussed later. The H_2S absorption cross section is also continuous and has a weak temperature dependence. The cross sections used here were measured at room temperature also (Robert Wu, private communication, 1995).

Analysis of the spectra to determine molecular abundances depends upon assumptions about the altitude distribution of the gases. We begin by considering a single-layer model in which the gases and aerosols are uniformly mixed. These models have the virtue of simplicity and also provide a calibration point for other modeling investigations. By adjusting the mixing ratios of CS_2, H_2S, and NH_3 we find the optimal fit with this simple model, shown in Fig. 7. The mixing ratios used in this model are listed as model A in Table III. There are several regions where the fit is poor, especially in the 194–200 nm spectral region. NH_3 absorbs strongly at 194, 197, and 200 nm, causing the model curves to lie below the observed reflectivity. It is not possible to correct this deficiency by adjusting the mole fraction of NH_3 because the models would then have too little absorption at 207 and 211 nm. Thus, we are led to the conclusion that the absorbing gases and aerosols are not uniformly mixed.

The fact that the NH_3 features are visible at 186, 213, and 216 nm, where the reflectivity is fairly high, but not

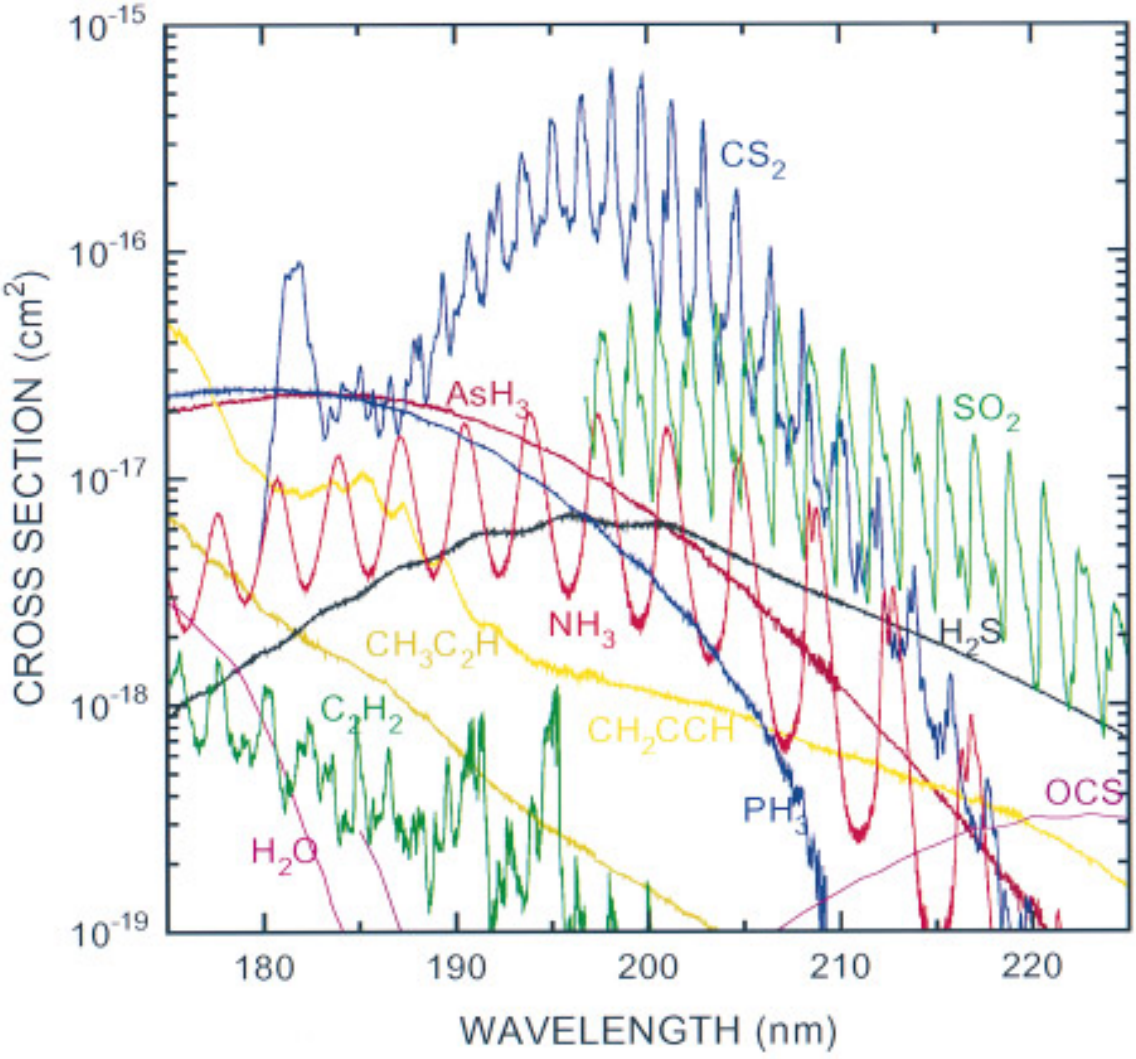

FIG. 4. The absorption cross section of the molecular species considered in this analysis. References for the absorption cross sections are listed in the text.

at wavelengths where the albedo is relatively low, suggests that the NH_3 is distributed to deeper pressures than CS_2. Essentially, because of the additional absorption due to CS_2, radiation in the 190–206 nm region penetrates to shallow depths in the atmosphere, while radiation at longer and shorter wavelengths probes deeper levels. Consistent with these intuitive expectations, we find that models with CS_2 lying above NH_3 and H_2S provide a much better fit to the spectra. In fact, the requirement for fitting the 197-nm features seems to be that there is a considerable optical depth of scattering aerosols between the layer containing CS_2 and the layer containing H_2S and NH_3.

Figure 8 shows results from a model with CS_2 confined to a thin, aerosol-free layer above the aerosol scattering layer. The fit is greatly improved near 194, 197, and 199 nm. The parameters describing this calculation are listed as model B in Table III. The base of the top layer is taken as 1 mbar and the aerosols are assumed to be distributed uniformly from 1 to 100 mbar. H_2S and NH_3 are uniformly distributed from 5 to 100 mbar. We find that H_2S and NH_3 must extend to pressures as small as 5 mbar to produce absorption features of the observed strength. The 1-mbar boundary between the top and middle layers is not well determined; it is possible to place the boundary at pressures larger by a factor of several, adjust other parameters slightly, and still fit the observations. It is also possible to place this boundary at any lower pressure as long as the column abundance of CS_2 is kept the same. The essential point is that the scattering depth in the top layer is very small (less than 1%); thus, CS_2 functions as an absorber above a reflecting layer and the spectrum is primarily sensitive to the CS_2 column abundance rather than the mole

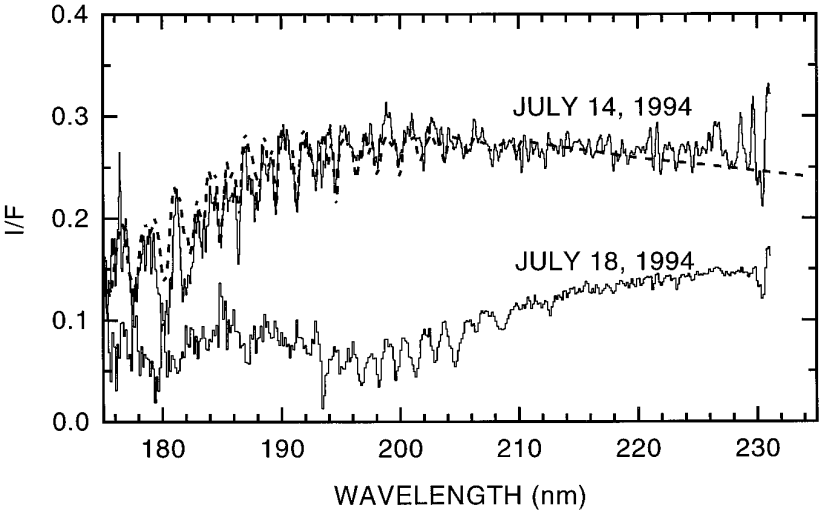

FIG. 5. A comparison of post- and pre-impact spectra obtained on July 14 and July 18, 1995. The observing geometry is Table I and is similar in the pre- and post-impact spectra. The pre-impact spectrum shows evidence for C_2H_2 absorption but not NH_3. Also shown is a synthetic spectrum based on a model atmosphere containing only H_2, aerosols, and C_2H_2.

fractions. For the parameters in model B the CS_2 column abundance is 1×10^{-7} g-cm^{-2}.

The primary deficiency of model B is the poor match between the calculations and observations at 193.5 nm. This wavelength coincides with the location of a solar Fraunhoffer line (see Fig. 1). The wavelength of this surprisingly strong absorption band is consistent with the CS_2 spectrum, but it is impossible to fit this feature with any CS_2 distribution. One possible explanation is that the feature is caused by a coincidence between a solar emission line and a CS_2 absorption line. If this were the case, then our division of low-resolution averages of the solar spectrum and CS_2 absorption spectrum would not give the proper reflectivity for the atmosphere. Careful examination of the solar spectrum reveals that there is an emission line at the center of the Fraunhoffer line, suggesting that a coincidence between a solar line and a CS_2 line is a possibility. However, we are unable to quantitatively test this hypothesis because the CS_2 spectrum is not known in sufficient detail to determine if there is in fact a coincidence between the solar emission line and CS_2 absorption line.

Uncertainties and non-uniqueness. The fit shown in Fig. 8 is excellent but the derived gaseous abundances still suffer from uncertainties related to imprecise knowledge of the absorption cross sections, the aerosol distribution, and the uniqueness of the fit. Uncertainties caused by the absorption cross sections occur primarily with CS_2.

The CS_2 absorption features in the range 190–210 nm are caused by absorption in the vibrational bands of the $^1\Sigma_g^+ \leftarrow {}^1B_2$ ($^1\Sigma_u^+$) transition (Douglas and Zanon 1964), which is complex and poorly understood. Lifetimes, linewidths, and the rotational structure of the bands have yet to be determined and therefore we are unable to perform a proper line-by-line synthesis of the CS_2 spectrum and must instead rely upon laboratory measurements of absorption cross sections. However, it is important to determine the level of uncertainty introduced by this approximation.

The spectral line nature of the CS_2 bands has two important consequences. First, the absorption cross sections of such bands tends to be temperature sensitive because changes in temperature affect the rotational and vibrational populations of the lower levels, causing changes in the line strengths. This same mechanism can also induce a temperature dependence (albeit usually a weak one) to continuum absorbers such as C_2H_2 (cf. Chen *et al.* 1991; Wu *et al.* 1989; Smith *et al.* 1991). Second, the saturation of the spectral lines can cause departures from Beers' law in low-resolution spectra.

Recent measurements of the CS_2 cross section have confirmed that it is temperature sensitive (Chen and Wu 1995). Figure 9 shows synthetic spectra calculated using cross sections measured at temperatures of 295 and 383 K. The 383 K cross section provides a significantly better match to the observations. In particular, the relative depths of the bands at 198 and 200 nm and at 203 and 205 nm are better matched by the 383 K cross section than the 295 K cross section. This suggests that the CS_2 in Jupiter's atmosphere may be at a relatively high temperature.

When analyzing low-resolution spectra, such as those presented here, the absorption properties of a molecular band formed from discrete lines differs from that of continuum absorbers like H_2S and NH_3 because of the need to average over the spectral line structure. These well-known

TABLE III
Model Runs

Pressure (mbar)	CS_2 (V/V)	H_2S (V/V)	NH_3 (V/V)	Aerosols $a(\mu m)$	k	$N(cm^{-2})$
			Model A, July 18, 1994			
0–100	2×10^{-9}	1×10^{-8}	2×10^{-8}	0.25	0.03	2×10^{9}
			Model B, July 18, 1994			
0–1	7×10^{-9}	—	—	—	—	—
1–5	—	—	—	0.25	0.03	0.1×10^{9}
5–100	—	5×10^{-8}	1×10^{-7}	0.25	0.03	1.9×10^{9}
			Model C, July 18, 1994			
0–1	7×10^{-9}	—	—	—	—	—
1–5	—	—	—	0.32	0.02	0.1×10^{9}
5–100	—	5×10^{-8}	1×10^{-7}	0.32	0.02	1.9×10^{9}
			Model D, July 18, 1994			
0–1	5×10^{-9}	—	—	—	—	—
1–5	—	—	—	0.25	0.035	2.5×10^{7}
5–100	—	2×10^{-8}	1.3×10^{-8}	0.25	0.035	4.75×10^{8}
			Model E, July 18, 1994			
0–1	5×10^{-9}	—	—	—	—	—
1–5	—	1.5×10^{-7}	1.5×10^{-7}	0.25	0.028	1×10^{9}
5–300	—	1.5×10^{-7}	1.5×10^{-7}	—	—	—
			Model F, August 9, 1994			
0–0.1	2×10^{-8}	—	—	—	—	—
0.1–1	—	—	—	0.25	0.031	2×10^{7}
1–100	—	—	1×10^{-7}	0.25	0.031	2×10^{9}
			Model G, August 23, 1994			
0–0.1	1×10^{8}	—	—	—	—	—
0.1–1	—	—	—	0.25	0.04	2×10^{7}
1–100	—	—	3×10^{-8}	0.25	0.04	2×10^{9}

''curve of growth'' effects have plagued many spectroscopic analyses (see Belton (1981) for a discussion of this problem in the analysis of SO_2 spectra). If we knew the wavelength, strength, and width of each spectral line we could calculate the absorption properties using standard techniques for the radiative transfer in molecular bands. However, our knowledge of CS_2 molecular structure is limited and we are unable to construct a spectral line list. Instead, we describe the CS_2 absorption properties with a Malkmus random band model. The Malkmus model is described in many standard texts including Goody and Yung (1989) and Liou (1992). Briefly, the Malkmus model describes the absorption in a molecular band in terms of two parameters, the mean line strength and the mean line spacing. We determine the mean line strength by requiring that the absorption cross section be equal to the laboratory measurements in the optically thin regime. We are then left with a family of models characterized by the value of the mean line spacing. The mean line spacing parameter may in some cases actually be related to the mean spacing between CS_2 spectral lines but it is probably best to simply view it as a simple way to parameterize our ignorance of the CS_2 absorption spectrum. If the mean line spacing is large, saturation is important, and the amount of CS_2 required to produce an absorption feature of a given depth is larger than the abundance derived with saturation neglected (i.e., assuming Beer's law).

Fortunately, saturation of the CS_2 absorption band appears to be a minor effect. Figure 10 shows a comparison of the July 18 spectrum with several models. The solid curve represents model B in Table III using the laboratory cross sections directly by assuming Beer's law. The dashed curve is based on a model atmosphere identical to model B, but using a Malkmus band model with a mean line spacing of 200 nm^{-1} to calculate the CS_2 absorption. The dotted curve represents calculations using the Malkmus

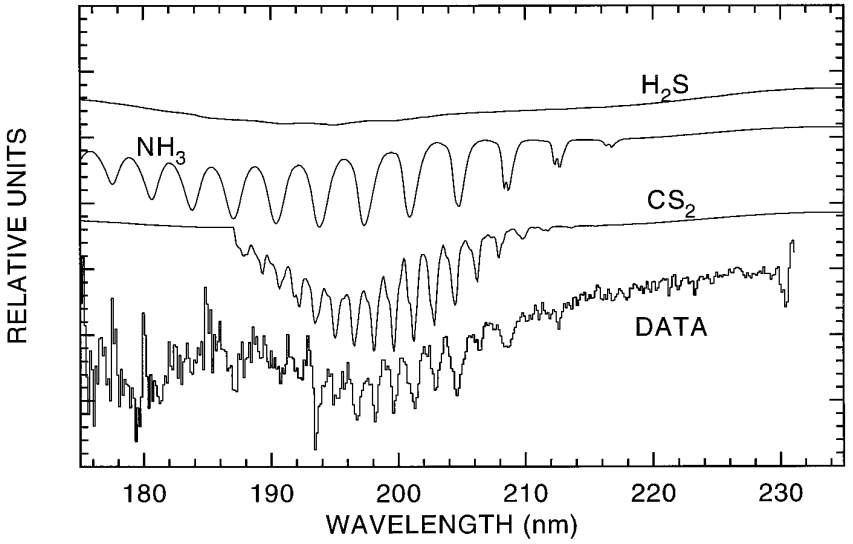

FIG. 6. The spectral signatures of the primary absorbers in the spectral range 175–230 nm. Throughout much of this wavelength region the absorption features of NH_3 and CS_2 are correlated except at 194, 197, and 199 nm where NH_3 has absorption maximum and CS_2 absorption minima.

band model and a mean line spacing of 200 nm^{-1} but with the CS_2 abundance increased by 30%. The fit is nearly as good as that of model B.

A mean line spacing of 200 nm^{-1} is probably lower than the actual mean line spacing. The CS_2 $^1\Sigma_g^+ - ^1B_2(^1\Sigma_u^+)$ band consists of dozens of vibrational bands, each possessing hundreds of rotational lines (Douglas and Zanon 1964, Hemley *et al.* 1983) and it is more likely that there are thousands of lines per nanometer rather than hundreds. For mean line spacings much larger than 200 nm^{-1} band saturation effects are unimportant for the column abundances considered here. Thus, we conclude that the poorly understood structure of the CS_2 $^1\Sigma_g^+ \leftarrow ^1B_2(^1\Sigma_u^+)$ band introduces uncertainties of less than 30% into our analysis.

Although H_2S does not possess any sharp spectral features which uniquely identify it, the arguments for a significant abundance in the atmosphere are strong. Figure 11 shows a comparison of a synthetic spectrum and the July 18 data. The synthetic spectrum is based on a model atmosphere which is identical to model B, except lacking

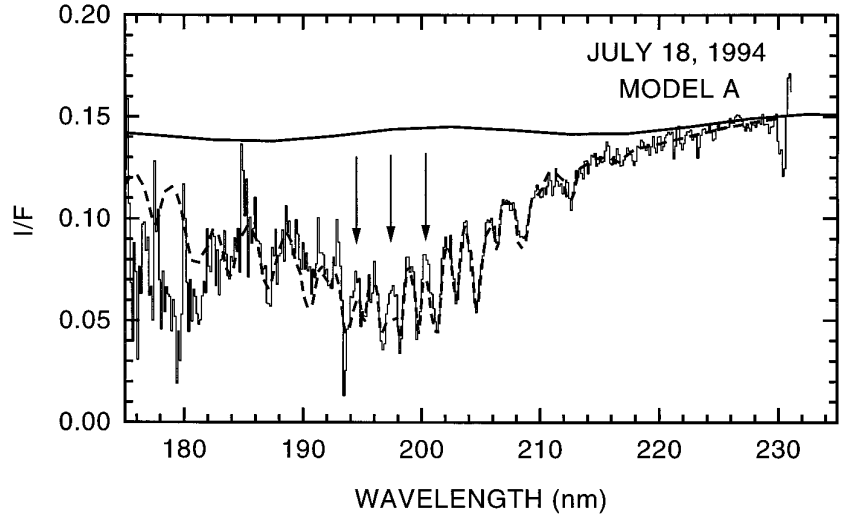

FIG. 7. Comparison of the July 18 spectrum with a single-layer model of the jovian atmosphere, listed as model A in Table III. The upper solid curve shows the reflectivity of an atmosphere containing only the aerosols in model A. The arrows indicate regions where the match between the model and observations is poor because of too much NH_3 absorption.

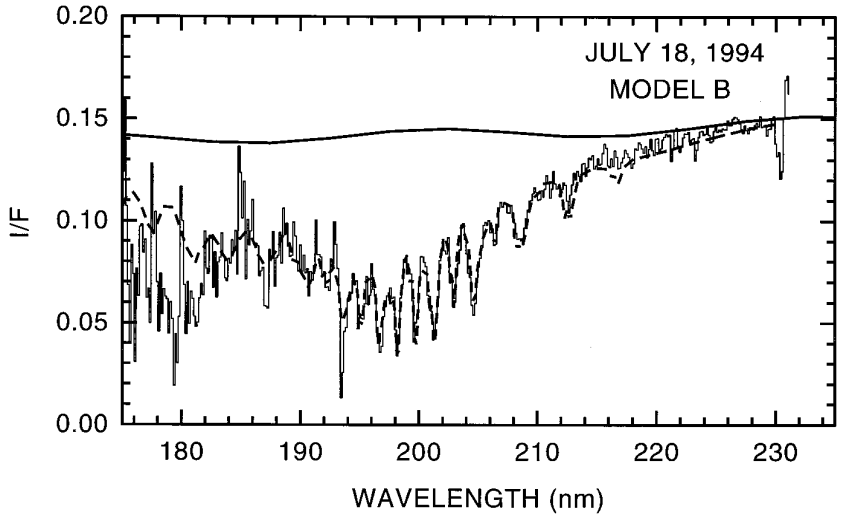

FIG. 8. Comparison of the July 18 spectrum with a three-layer model of the jovian atmosphere, listed as model B in Table III. The upper curve shows the reflectivity of an atmosphere containing only the aerosols in model B. This model represents our best fit to the July 18 spectrum.

H_2S. The fit in the 210–230 nm wavelength region is poor. The agreement cannot be improved by increasing the abundance of NH_3 or CS_2 because neither of these molecules has a significant absorption cross section in the 210–230 nm wavelength region. We know of no other molecules that possess absorption cross sections of the proper shape; however, the list of potential absorbers is infinite and we have not checked them all. We have examined the set of absorbers shown in Fig. 5 and among this set of potential absorbers H_2S is the only choice. It is also an excellent choice, providing a very good match to the observations. Essentially what is required is a molecule with a peak in its absorption cross section in the ~200 nm region. Although molecules such as CH_3C_2H and AsH_3, have the right shape in the 210–230 nm region, they produce too much absorption at wavelengths shortward of 200 nm.

We also consider it unlikely that the slope in the region 210–230 nm is due to aerosols. None of the aerosol models considered by us exhibit spectral variations that are consistent with the observed spectra. The best candidate is shown in Fig. 12 and is based on model C in Table III. We have adjusted the aerosol properties to match the slope in the 210–230 nm region but the model predicts too low a reflectivity shortward of 194 nm. The features at 197 and 200

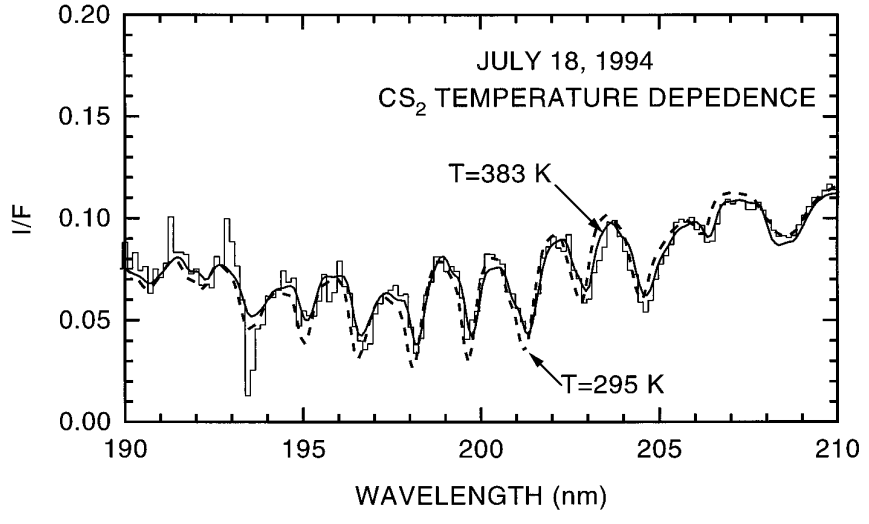

FIG. 9. A comparison of synthetic spectra calculated using the CS_2 cross section at two different temperatures. The observations are better matched by the cross section at 383 K.

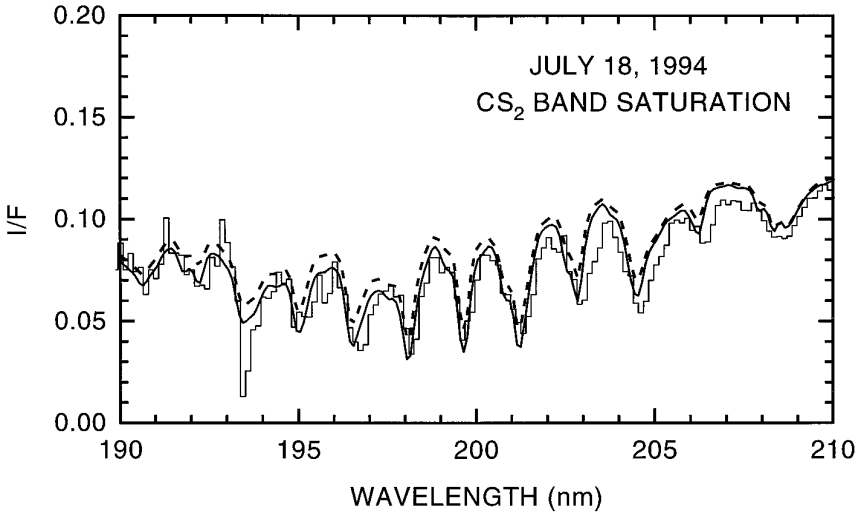

FIG. 10. This figure shows the effects of saturation of spectral lines on the CS_2 absorption spectrum. The histogram represents the data from July 18 and the solid line model B from Table III. The dashed line shows the spectrum calculated from model B using a Malkmus band model for CS_2, as described in the text. The dotted curve is also based on model B and a Malkmus band model but the CS_2 abundance has been increased by 30%.

nm are not well fit either. To produce an improved fit requires adoption of a wavelength-dependent imaginary index of refraction. Although there is no physical reason to discount this possibility, we see little value in constructing aerosol models which mimic the absorption properties of H_2S. Moreover, as we will show, the August 9 data exhibit no evidence for H_2S absorption (i.e., the reflectivity is flat from 210 to 230 nm). This change in the character of the spectrum can be easily explained by hypothesizing that H_2S is not longer present in the upper atmosphere (because of photochemical destruction, for example). If we were to attribute the slope in the 210–230 nm region to aerosols alone, then we would be forced to conclude that the optical properties of the aerosols changed to become less absorbing at shorter wavelengths. This seems unlikely.

Figures 13 and 14 show calculations which explore the uncertainties in the inferred gas composition caused by uncertainties in the aerosol models. Models D and E employ different aerosol distributions than model B and are therefore useful to judge the sensitivity of the gas results to the aerosol model. The structure of models D and E is similar to that of model B in that the CS_2 is placed in a thin layer at low pressure above the aerosols and H_2S and NH_3. The abundance of CS_2 varies by less than 30% in both

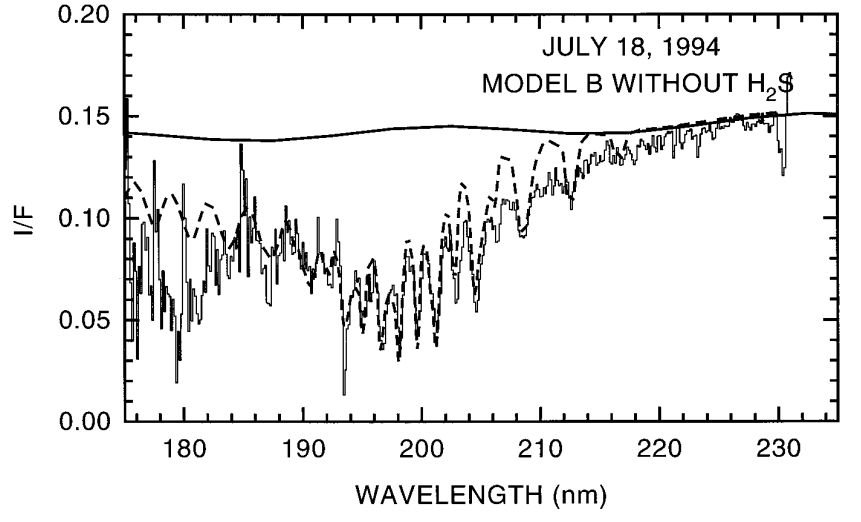

FIG. 11. The effect of H_2S on the synthetic spectrum based on model B.

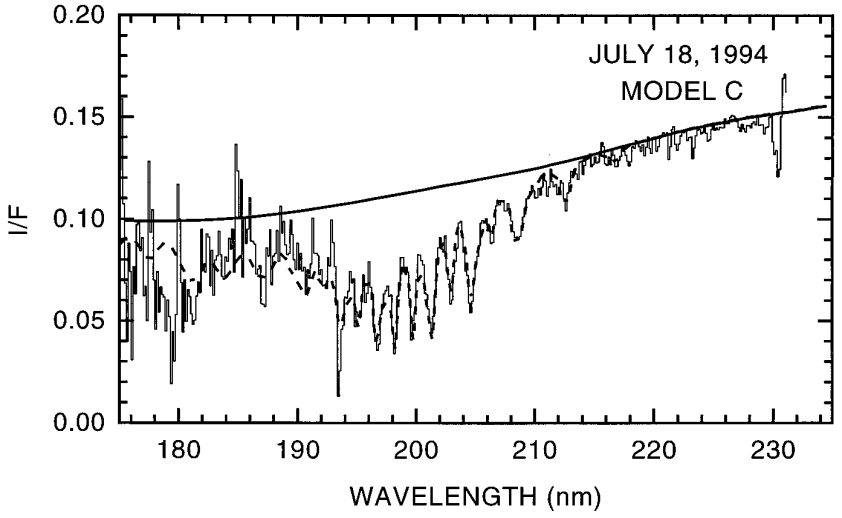

FIG. 12. Comparison of the July 18 data with model C in Table III. In this model we have adjusted the aerosol properties to fit the 210–230 nm region. The fit is poor at shorter wavelengths. To fit the entire spectrum without H_2S requires that the aerosol properties, primarily k, vary in a manner which mimics H_2S absorption.

cases. This is to be expected because the CS_2 abundance is fixed by the band depths and the details of the aerosol distribution matter little as long as the aerosol layer reflects the proper amount of UV light. The slight change in the CS_2 abundance in these models is attributable to the fact that the slope of the gas-free spectrum varies with the aerosol models.

According to model E, the mole fractions of H_2S and NH_3 do not depend strongly on the altitude distribution of the aerosols. Confining the aerosols to the 1- to 5-mbar level changes the mole fractions of H_2S and NH_3 by factors of 2 and 7. Altering the optical properties of the aerosols produces larger changes in the mole fractions, as shown in model D. Both models D and E are significantly worse fits to the data than model B, especially at 197 nm; therefore, these examples probably limit the range of acceptable values for the H_2S and NH_3 mole fractions. Thus, the NH_3 mole fraction is determined to within an order of magnitude and the H_2S mole fraction to within a factor of 3.

Upper limits on SO_2, H_2O, C_2H_2 OCS, and SO. SO_2 has a prominent absorption band system in the UV spectral range (Mannatt and Lane 1994), and its presence might

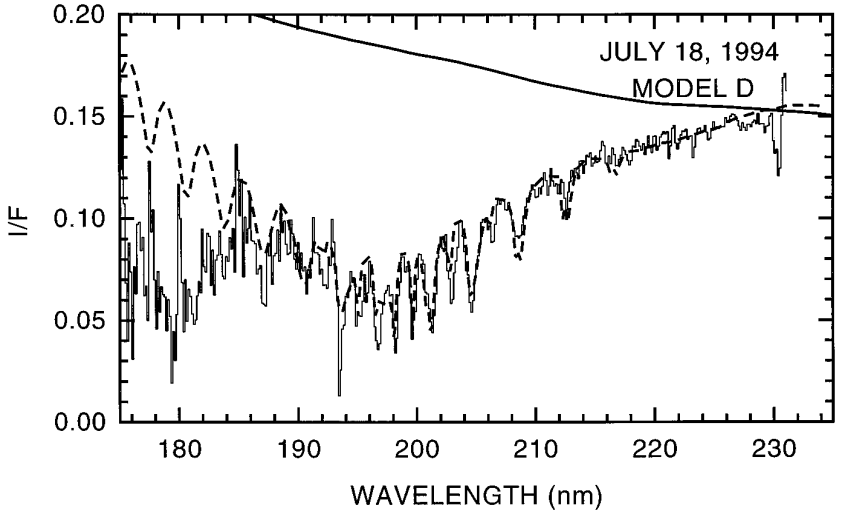

FIG. 13. Comparison of the July 18 spectrum with model D in Table III. The upper solid curve shows the reflectivity of an atmosphere containing only the aerosols in model D.

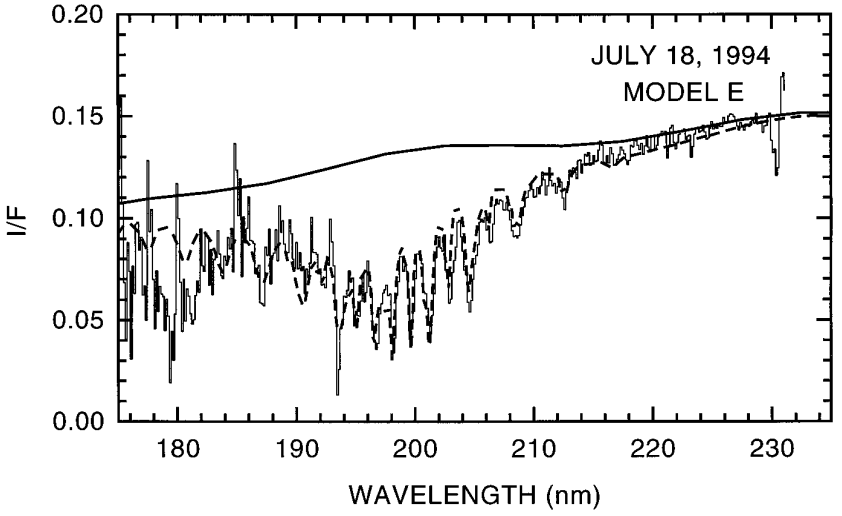

FIG. 14. Comparison of the July 18 spectrum with model E in Table III. The upper curve shows the reflectivity of an atmosphere containing only the aerosols in model D.

be expected based on the detection of other sulfur-bearing molecules and the distinct possibility that H_2O from the comet or jovian atmosphere participated in the chemistry that produced the other sulfur-bearing molecules; nevertheless, our spectra show no sign of SO_2. To obtain an upper limit to the SO_2 abundance we use model B and add varying amounts of SO_2, assuming that it has the same altitude distribution as CS_2. We find that a SO_2 mole fraction of 10^{-8} produces spectral features in the model which are clearly not present in the data and therefore adopt this value as our upper limit. A mole fraction of 10^{-8} corresponds to a column abundance of 10^{-7} g-cm^{-2}. We have calculated similar models with SO and derive an upper limit of 3×10^{-7} g-cm^{-2}.

OCS emissions from the K+W impact site have been detected at microwave wavelengths (Lellouch *et al.* 1995) and we have search for evidence of it in the FOS spectra. Unfortunately, its absorption cross section is small and the upper limits we derive are correspondingly large. Assuming that it is also co-located with CS_2 we estimate an upper limit of 10^{-5} g-cm^{-2}.

None of the models presented so far adequately fit the observed spectra at wavelengths less than 185 nm. As discussed earlier, the reliability of the G190H spectra is poor at these wavelengths. In addition, there are no easily identifiable spectral features to guide our analysis. Moreover, the list of potential absorbers at these wavelengths is endless: it includes moderately complex hydrocarbons (C_2H_2, C_2H_4, C_4H_2, CH_3C_2H, ...) PH_3, AsH_3, and others. If oxygen and sulfur compounds are added to the list, the situation becomes totally unmanageable. Quantitative analysis of this region of the spectrum will not be highly rewarding without further observational or theoretical guidance. Nevertheless, we consider below two potential absorbers.

A particularly important absorber might be H_2O, given its large abundance in comets and in the deep jovian atmosphere. Figure 15 shows models including H_2O in the 5- to 100-mbar layer. The models with H_2O do not reproduce the shape of the *I/F* curve at wavelengths of less than 180 nm very well; however, as discussed earlier this region is affected by scattered light subtraction. An H_2O mole fraction of 10^{-6} reproduces the slope of the *I/F* curve from 180 to 185 nm, but then we seriously underestimate the reflectivity at 175 nm. If the upturn from 180 to 175 nm is real, then it implies that the mole fraction of H_2O in the stratosphere is less than 3×10^{-7}. If the upturn is not real, then the H_2O mole fraction could be as high as 10^{-6}.

As mentioned above, the pre-impact spectrum obtained on July 14 shows clear evidence for C_2H_2. The post-impact spectra, however, do not show any features readily identifiable as C_2H_2 absorption. This may be due in part to the lower reflectivity of the post-impact spectra. The models are in fact able to accommodate relatively large mole fractions of C_2H_2 without departing seriously from the observations and in some cases adding C_2H_2 results in a better fit. Figure 16 shows a comparison of the July 18 data with a model that is identical to model D but with the addition of C_2H_2 distributed uniformly throughout the atmosphere with various mole fractions. Model D was chosen for this illustration because the aerosol distribution used in this model causes a relatively high reflectivity at short wavelengths. Adding C_2H_2 lowers the reflectivity shortward of 190 nm, bringing the model closer to the observations.

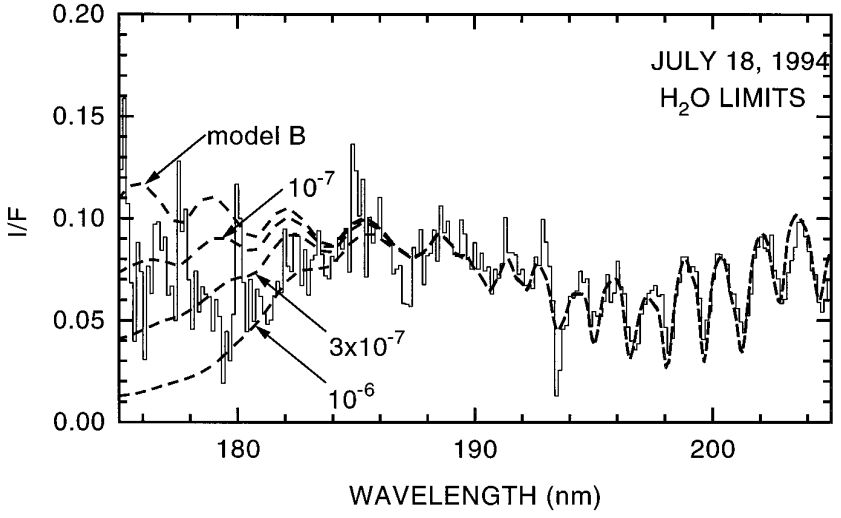

FIG. 15. Comparison of the July 18 spectrum with a model including H_2O. The model is identical to model B in Table III except that H_2O has been included with a uniform altitude distribution. Curves are shown for several different mole fraction of H_2O. Inclusion of H_2O improves the quality of the fit at short wavelengths.

Spectra from August 9 and 23. The spectra obtained on August 9 and 23 differ from that obtained on July 18 in that, while CS_2 and NH_3 are still obviously present, there is no evidence for H_2S absorption. Figure 17 shows a fit to the August 9 spectrum (Model F in Table III). A few features are noteworthy. First, we are able to fit the August 9 data with essentially the same aerosol model that fit the July 18 data, suggesting that temporal and spatial variations in the aerosol distribution between the two observations are minor. Second, the CS_2 column abundance is roughly a factor of 3 less than on July 18, while the NH_3 column abundance is the same; however, in order to fit the spectrum in the 197 nm region, we find that the CS_2 must be confined to pressures of less than $\approx$0.1 mbar. This is a significant finding. Because these observations occurred near the limb they probe to higher levels in the atmosphere than the July 18 observations. The July 18 observations in fact only constrain the CS_2 to lie above 1 mbar, so it is entirely possible, and perhaps likely, that CS_2 is confined to pressures less than at least $\approx$0.1 mbar on all dates. If our conclusions regrading the high temperature are correct, then they imply that CS_2 resides in the uppermost

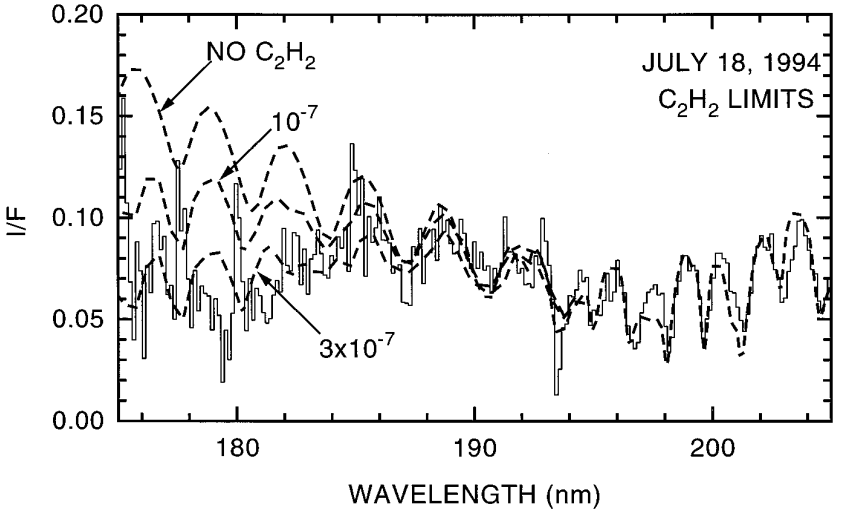

FIG. 16. Comparison of the July 18 spectrum with a model including C_2H_2. The model is identical to model B in Table III except that C_2H_2 has been included with a uniform altitude distribution. Curves are shown for several different mole fractions of C_2H_2. Inclusion of C_2H_2 improves the quality of the fit at short wavelengths.

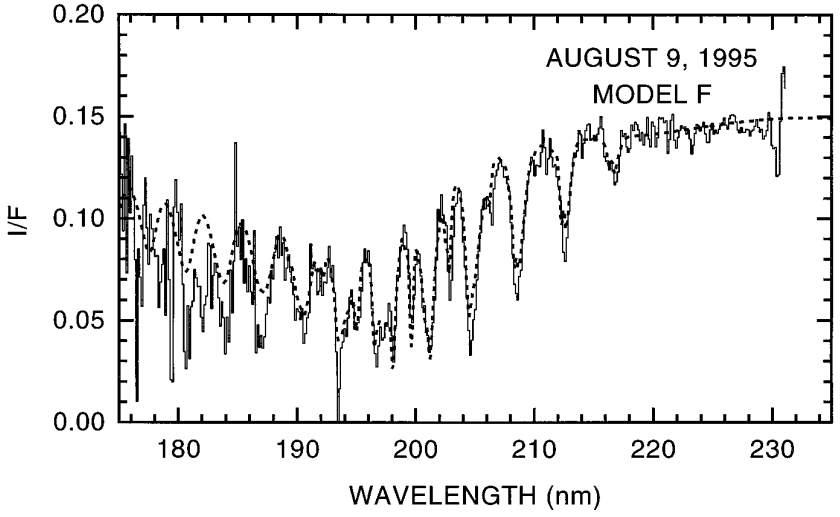

FIG. 17. Comparison of the August 9 spectrum with model F in Table III. This spectrum shows no evidence for H_2S absorption. The altitude distribution of absorbers appears similar to that required to fit the July 18 spectrum; however, it is necessary to confine CS_2 to pressures of less than 0.1 mbar. The abundance of NH_3 has not changed, but CS_2 has decreased slightly.

portion of the stratosphere, probably near 1 μbar, where the thermospheric temperature increase begins.

Figure 18 shows a comparison of the August 23 spectrum with model G. An aerosol distribution different from that used to fit the July 18 and August 9 spectra are required to fit the August 23 spectrum. We match the spectrum in the region 220–230 nm by increasing the imaginary index of refraction from 0.03 to 0.04. West *et al.* (1995) found some evidence that the aerosol size increased with time but we are unable to fit the August 23 spectrum with aerosols having radii larger than $a = 0.25$ μm. The reason for this disagreement is not clear. The CS_2 absorption features in the August 23 spectrum imply that the density has decreased by another factor of two from August 9 and roughly a factor of 5 from July 18. The NH_3 abundance has also decreased by a factor of 3 from the earlier dates. Of course, the August 23 spectra were obtained at a different longitude than the other observations and part of the variation is likely due to this fact.

Spatial variations. It is important to remember that the spatial distribution of absorbing species is not determined by our observations. In the analysis we have assumed that the absorbers are distributed uniformly within our field of view, but the actual situation is unlikely to be that simple. Visible perturbations of the atmosphere, caused by increased aerosol content, are seen over areas with scales of 10,000 km in the visible images (Hammel *et al.* 1995). The gaseous absorbers could extend that far, but it may be unwise to assume that the gas and aerosols have similar distributions. On the other hand, the gaseous absorbers must occupy a significant fraction of the FOS field of view in order to produce the observed absorption features. Thus, the horizontal scale over which the absorbing gases are distributed is unlikely to be less than 3000 km or greater than 10,000 km.

IV. COMPARISON WITH OTHER RESULTS

The HST FOS spectra obtained on July 18, 1995 have been analyzed independently by Noll *et al.* (1995) and Atreya *et al.* (1995). There appear to be serious errors in Atreya *et al.*'s analysis which invalidate their results (Yelle and McGrath 1995). As a consequence, we discuss them no further. Noll *et al.* (1995) use reflecting layer models for the atmosphere and deduce column abundances of 0.5×10^{16} to 2.0×10^{16} cm^{-2} for NH_3, 0.5×10^{15} to 2.0×10^{15} cm^{-2} for CS_2, and 2×10^{16} to 5×10^{16} cm^{-2} for H_2S. Our estimate for the CS_2 abundance on July 18, 1994 is within the range determined by Noll *et al.*. The abundances for NH_3 and H_2S are difficult to compare. According to our results, most of the NH_3 and H_2S is beneath or mixed with the aerosols and in this case the reflectivity of the atmosphere is sensitive to the mole fraction of NH_3 and H_2S rather than the column abundance.

NH_3 has been observed in the infrared at the K and L impact sites with properties that are roughly similar to those derived here. The IR spectral emissions from the K impact site can be matched with a NH_3 mole fraction of 8×10^{-8} (Orton *et al.* 1995), which is close to our derived value of 1×10^{-7} in model B. Further analysis of the infrared observations by Griffith *et al.* (in preparation) indicates that the NH_3 mole fraction could be as high as 10^{-6} depending upon the thermal profile and altitude distribution of the gas. These authors also find that the NH_3

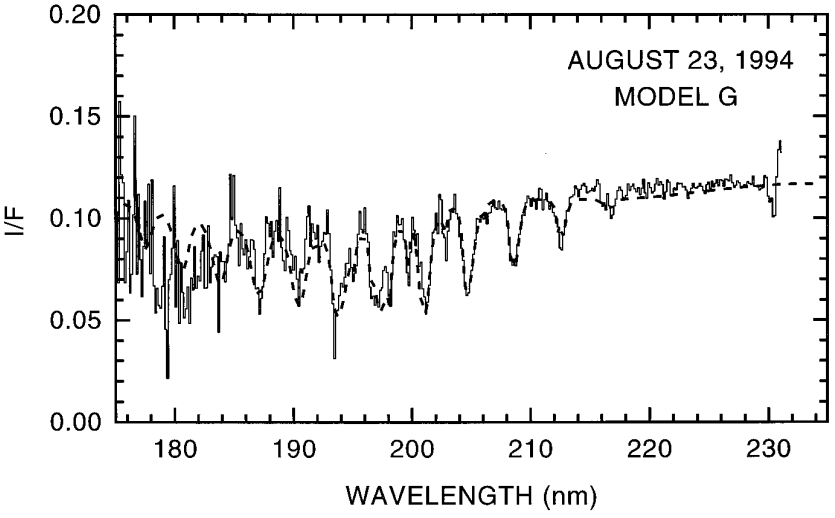

FIG. 18. Comparison of the August 23 spectrum with model G in Table III. The abundance of CS_2 has decreased even further and NH_3 has decreased by a factor of 3 from August 9.

abundance decreases sharply with distance from the impact site. Thus, there are no obvious conflicts with the UV analysis presented here. Analysis of high-resolution heterodyne observations of the Q1 impact site indicates that NH_3 is distributed from 1 to 30 mbar with a mole fraction for NH_3 of 1×10^{-8} (Orton *et al.* 1995). The fact that the NH_3 distribution determined from the heterodyne measurements extends to pressures as deep as 30 mbar is consistent with the conclusions presented here that NH_3 lies at relatively deep pressures.

Analysis of millimeter-wave observations reveal a number of species not normally present on Jupiter in significant abundance including HCN, CO, CS, and OCS (Lellouch *et al.* 1995, Marten *et al.* 1995). All of these molecules appear to reside at fairly low pressures. Marten *et al.* (1995) deduce from the width of the HCN line that the HCN is confined to pressures of less than 0.1 mbar, while Lellouch *et al.* (1995) find that the CO resides at pressures of less than ≈0.3 mbar. Thus, it appears that CS_2, HCN, CO, and CS are all present at the G impact site at pressures of less than a few tenths of a millibar and that OCS is present at roughly the same pressure at the K+W impact site. However, CS_2 appears to be less abundant than the other species. Assuming that CS_2 is distributed over an area 10,000 km in diameter surrounding the G impact site implies a total mass of 10^{11} g, whereas Lellouch *et al.* (1995) report masses of 10^{14} g of CO, 6×10^{11} g of CS, and 5×10^{12} g of OCS (at the K+W impact site), and Marten *et al.* (1995) infer a mass of 10^{12} g of HCN.

There do not appear to be any significant inconsistencies between the UV and millimeter-wave results. For example, Lellouch *et al.* estimate an OCS mass of 5×10^{12} g within their field of view. Assuming an emitting area for the millimeter lines with a diameter 10,000 km implies a column abundance of 6×10^{-6} g-cm^{-2}, which is below our upper limit of 10^{-5} g-cm^{-2}. Lellouch *et al.* (1995) do not detect H_2S and place an upper limit of $\approx 4 \times 10^{-6}$ g-cm^{-2} at the G impact site on July 19. Assuming that H_2S detected by HST is distributed uniformly from 5 to 100 mbar with a mole fraction of 10^{-7} implies a column-integrated mass of $\approx 2.5 \times 10^{-5}$ g-cm^{-2}, significantly larger than Lellouch *et al.*'s upper limit. However, the UV measurement and IR upper limit are not necessarily inconsistent because Lellouch *et al.* assumed that the H_2S was co-located with the other foreign species in the 0–0.1 mbar region, whereas our results indicate that H_2S resides at deeper pressures. In fact, Lellouch (1996) has computed an upper limit assuming that the H_2S lies at deep pressures and finds that in this case the upper limit is greater than the abundance deduced here. There is also the possibility of temporal variations since the IR measurements used to search for H_2S were performed ≈1 day after the UV observations.

V. DISCUSSION

Our goal is to use the characteristics of the aerosols and gaseous absorbers derived in the previous sections to investigate the physical nature of the impact. Although there are numerous uncertainties related to the assumptions in our models, we have several solid results. The identification of CS_2 and NH_3 is unambiguous and the column abundance of CS_2 within the FOS field of view is well determined. Although they possess no sharp spectral features, the FOS spectra are best fit by models containing H_2S; additionally, the differences between the July 18 spectra and later spectra argue strongly for the presence of

H_2S on July 18. In what follows we consider the detection of H_2S to be definite. CS_2 resides at a lower pressure than the other gaseous absorbers and the aerosols. The mole fractions of H_2S and CS_2 are not well determined (because of uncertainties in the aerosol properties) but appear to be on the order of 10^{-7}. Finally, the abundance of all three gaseous absorbers decreases with time, each at a different rate. Despite the uncertainties in the models these facts provide some important insight into the response of the jovian atmosphere to the impacts.

Two Sources for Foreign Species

We have established that on July 18 and August 9 CS_2 is present at relatively high levels in the atmosphere, compared with H_2S, NH_3, and the aerosols. This is probably also true for the August 23 observations, although the evidence is less strong there. For the August 9 data we find that CS_2 must reside at pressures of less than 0.1 mbar, and there is no reason to believe that CS_2 is at deeper pressures on the other dates. On the other hand, the distribution of aerosols, H_2S, and NH_3 must extend to pressures greater than $\approx$5 mbar. The different altitude distributions of these constituents suggest different origins.

CS_2 has not been previously detected on Jupiter and is not thought to be present in significant abundance (Fegley and Lodders 1994). H_2S has not been detected but is believed to be present below the NH_4–SH clouds. The abundance of H_2S, which is also essentially the sulfur abundance in the atmosphere, is not known. The solar abundance is 3.8×10^{-5}, but microwave observations of NH_3 have been used to argue for an abundance roughly 6–7 times solar (de Pater, 1991) at levels below the NH_4–SH cloud. H_2S should not be present with any significant abundance above the NH_4–SH cloud (Lewis 1969, Larsen *et al.* 1984). NH_3 in the jovian atmosphere has been extensively studied and is known to have a mole fraction of $\approx 10^{-7}$, set by saturation at the tropopause (i.e., roughly 100 mbar), and to decrease rapidly because of photochemical loss at higher altitudes (cf. West *et al.* 1986). The solar abundance of NH_3 is 1.7×10^{-4}, but it is likely that the abundance in the deep atmosphere below the NH_4–SH cloud is somewhat higher (de Pater 1991, Fegley and Lodders 1994). Given these characteristics, it is tempting to construct the following simple picture.

CS_2, as a truly foreign species, must be created by thermally driven chemistry in the plume or in the ''re-entry'' shock when the plume material falls back on the atmosphere (Zahnle *et al.* 1995). Thus, CS_2 will either be created or deposited at relatively low pressures in the jovian atmosphere, as will the other foreign species CS, OCS, HCN, and CO. While it is possible that H_2S and NH_3 are also transported from the reservoirs deep in the atmosphere to the stratosphere by the plume, the fact that these species reside at deeper pressures than CS_2 argues against this possibility. Rather, it seems more likely that H_2S and NH_3 have been carried into the lower stratosphere by upwelling associated with the impact. This mild, large scale upwelling should be differentiated from the highly energetic, narrowly confined plume seen in the HST images.

The mix of cometary and jovian gas seen in the plume will spread out and descend back onto the atmosphere, eventually stopping at a level where the pressure of the ambient gas is sufficient to absorb the momentum of the falling gas. Numerical estimates imply that the infalling gas will be stopped at pressure levels significantly less than 0.1 mbar (Zahnle *et al.* 1995). Our results, on the other hand, imply that H_2S and NH_3 reside at deeper levels in the atmosphere. The foreign species could not have been carried to deeper pressures by diffusion or eddy mixing because the transport times are far too long. Typical time scales for vertical transport in a stratosphere are on the order of months to years, yet H_2S and NH_3 were detected 3 hours after impact. Neither can we conjecture that vertical mixing was greatly enhanced over the usual values by the impact because NH_3 is seen to persist for many weeks, indicating that the transport times in the disturbed atmosphere are at least that long. Thus, it is very difficult to understand how NH_3 and H_2S could be present in the lower stratosphere if these species were deposited at low pressure by the falling plume.

The alternative to delivery from above is upwelling from below. We propose that the H_2S and NH_3 observed by HST were carried to the stratosphere by convection caused by heating of air in the region between the NH_4–SH and H_2O clouds. The ambient jovian air could be heated by radiation produced in the explosion or by sound waves. If the base of the convecting region is at 2 bars and its temperature is raised by 5 K by the explosion then roughly 10^{25} ergs are required. This is a small fraction of the total energy involved in the explosion.

The hypothesis of large-scale upwelling near the G impact site may also help to explain another aspect of the HST observations. West *et al.* (1995) have shown that the aerosols at the G impact site extend to pressures at least as deep as 100 mbar. They also show that aerosols with radii of 0.25 μm have settling times on the order of weeks to months. Yet, the aerosols appear to be at 100 mbar within hours after the impact. If the aerosols are deposited on the top of the atmosphere by the plume they should not be present at 100 mbar shortly after the impact. The alternative is that they are brought up to the stratosphere by upwelling from below.

If NH_3 and H_2S are transported to the stratosphere by upwelling then they must be carried there in the form of ice crystals rather than vapor. The amount of energy available appears capable of heating the jovian atmosphere over large distances by a small amount but should not

perturb the usual temperature profile to a degree that would inhibit NH_3 and H_2S condensation, i.e., the tropopause should still be intact though its temperature may differ from the usual value by a small amount (Orton *et al.* 1995). As a consequence the upwelling must be vigorous enough and the ice crystals must be small enough so that they are carried through the tropopause to the stratosphere where they sublime at relatively high temperatures. A similar mechanism has been suggested for carrying the condensable CH_4 into the stratosphere of Neptune (Lunine and Hunten 1989).

Oxygen and the Impact Depth

The lack of SO_2 implies that the plume material participating in the thermal chemistry and carried to the upper atmosphere was lacking in oxygen. According to Zahnle *et al.* (1995) chemistry occurring in the fireball and in the re-entry shock should produce significantly more SO_2 than CS_2 if the air has a solar abundance of H_2O. The simplest explanation for the lack of SO_2 is that the G fragment penetrated the NH_4–SH cloud but not the H_2O cloud, which resides at roughly 5 bars (Larson *et al.* 1984). This, in turn, places constraints on the mass of the impactor. The NH_4–SH cloud base is at 2 bars (Larson *et al.* 1984). Assuming a density of 0.6 g-cm^{-3} (Asphaug and Benz 1994) and using Eq. (5) in MacLow and Zahnle (1994) implies a diameter for the impactor of 0.5–1.0 km for penetration to 2–5 bars. It may also be possible that the impactor penetrated to greater depth, but the material injected into the upper atmosphere was predominantly from the 2–5 bar region.

Temporal Variations

The differences between the spectra on July 18, August 9, and August 23 are suggestive of temporal variations. In principle, it is possible that some of the differences could be due to the fact that slightly different regions of the planet were observed, but we have insufficient data to address this possibility. In the future, more detailed models of the impacts and other observations may help remove this ambiguity. For now, we will try to understand what types of temporal variations are possible and how they relate to the observations. In principle, CS_2, H_2S, and NH_3 could be lost through transport out of the stratosphere or through chemical processes. We investigate the latter possibility because vertical transport times in the stratosphere are typically very long.

The lifetimes of solitary H_2S and NH_3 molecules in free space at 5.2 AU are 0.8 and 1.2 days, respectively. In the jovian atmosphere the average lifetime of these molecules is likely to be much longer because of the diurnal cycle, because an individual molecule may be shielded from solar UV by other molecules or by aerosols, and because the products of H_2S or NH_3 photolysis may combine to reform the original molecules. Diurnal averaging lengthens the photolysis lifetime by a factor of 2. Shielding by other molecules is also important. For the abundances derived here both NH_3 and H_2S are present at a level of about optical depth unity in the stratosphere; therefore, self-shielding may lengthen the photolysis lifetime by another factor of 2. Shielding by aerosols contributes another factor of 2. According to West *et al.* (1995), only 25% of NH_3 photolysis events result in irretrievable destruction of the molecule. According to Moses *et al.* (1995a) H_2S is not efficiently recycled. Thus, the effective lifetime against photolysis for both NH_3 is on the order of 1 month and H_2S is on the order of 1 week. Moses *et al.* (1995a, b), using detailed chemical models, calculate lifetimes which are consistent with these simple estimates. These estimated lifetimes are consistent with our observations which show H_2S to be absent 22 days after the impact and NH_3 to be decreasing 36 days after the impact.

CS_2 exhibits the most interesting variation with time because all three dates show different abundances. According to Moses *et al.* (1995a), CS_2 has a photolysis lifetime of 8 hr at low pressures. Shielding by other absorbers should be minor because CS_2 appears to reside at higher altitudes. Moses *et al.* (1995a) also argue that CS_2 will be recycled subsequent to photolysis and that it will be created through the reaction of sulfur atoms, liberated in S_2 photolysis, with hydrocarbon radicals. Moses *et al.* (1995a) estimate a lifetime of CS_2 of about 1 month, which is roughly consistent with our observations. Moses *et al.* also predict that, because of production from S_2, the CS_2 abundance will increase after several months. Observations of the impact sites once Jupiter is again observable with HST in February 1995 will test this prediction.

V. SUMMARY

The results from our analysis of FOS spectra may be summarized as follows:

(1) The spectra are well fit by aerosols, with properties similar to those derived from the imaging results and the gaseous absorbers CS_2, H_2S, and NH_3.

(2) The CS_2 column abundance in the FOS field of view 3 hr after the G impact is about 6×10^{-8} g-cm^{-2}. Moreover, the CS_2 lies above the bulk of the aerosols and H_2S and NH_3. CS_2 must be confined above at most a few millibars to fit the July 18 spectrum and a few tenths of a millibar to fit the August 9 spectrum.

(3) On July 18 the mole fractions of H_2S and NH_3 are comparable and of order 10^{-7}.

(4) Evidence for H_2S is absent on August 9 and August 23. The CS_2 abundance decreases by a factor of 2–3 from July 18 to August 9 and again by a factor of 2 from August 9 to August 23.

(5) The absence of SO_2 absorption features limits the abundance of SO_2 to less than 10^{-7} g-cm^{-2}, assuming that SO_2 has an altitude distribution similar to CS_2. H_2O may be present with a mole fraction of up to 1×10^{-7}. For some aerosol models the quality of the model fits are improved if C_2H_2 is included with a uniform altitude distribution and a mole fraction of 3×10^{-7}.

These characteristics, and the fact that NH_3 and H_2S are present in the deep jovian atmosphere, suggest that CS_2 has a different origin than the other two molecules. We hypothesize that NH_3 and H_2S are brought to the stratosphere by upwelling from below caused by heating of ambient jovian air over a region on the order of thousands of kilometers. Further data analysis and modeling can test this hypothesis.

REFERENCES

Anders, E., and N. Grevese 1989. Abundance of the elements: Meteoritic and solar. *Geochim. Cosmochim. Acta* **53,** 197–214.

Asphaug, E., and W. Benz 1994. Density of comet Shoemaker–Levy 9 deduced by modelling breakup of the parent 'rubble pile.' *Nature* **370,** 120–124.

Atreya, S. K., S. G. Edgington, L. M. Trafton, J. J. Calswell, K. S. Noll, and H. A. Weaver 1995. Abundances of ammonia and carbon disulfide in the jovian stratosphere following the impact of comet Shoemaker–Levy 9. *Geophys. Res. Lett.* **22,** 1625–1628.

Belton, M. J. S. 1982. An interpretation of the near-ultraviolet absorption spectrum of SO2: Implications for Venus, Io, and laboratory measurements. *Icarus* **62,** 149–165.

Boslough, M. B., D. A. Crawford, A. C. Robinson, and T. G. Trucano 1994. Mass and penetration depth of Shoemaker–Levy 9 fragments from time resolved photometry. *Geophys. Res. Lett.* **21,** 155–1558.

Chen, F. Z., D. L. Judge, C. Y. R. Wu, and J. Caldwell 1994. Low and room temperature photoabsorption cross sections of NH_3 in the UV region. *Astrophys. Space Sci.,* submitted.

Chen, F. Z., D. L. Judge, C. Y. R. Wu, J. Caldwell, H. P. White, and R. Wagener 1991. High resolution, low temperature photoabsorption cross section measurements of C_2H_2, PH_3, AsH_3, and GeH_4, with application to Saturn's atmosphere. *J. Geophys. Res.* **96,** 17,519–17,527.

Chen, F. Z., and C. Y. R. Wu 1995. High-, room-, and low-temperature photoabsorption cross sections of CS_2 in the 1800–2300 Å region. *Geophys. Res. Lett.* submitted.

Chevalier, R. A., and C. L. Sarazin 1994. Explosions of infalling comets in Jupiter's atmosphere. *Astrophys. J.,* **429,** 863.

Clarke, J. T., R. Prange, G. Ballester, J. Trauger, D. Rego, R. Evans, K. Stapefield, W. Ip, F. Paresce, J-C. Gerard, H. Hammel, M. Ballav, L. Ben Jaffel, J-L. Bertaux, D. Crisp, C. Emerich, W. Harris, M. Horanyi, S. Miller, A. Storrs, and H. Weaver 1995. Hubble Space Telescope far-ultraviolet imaging of Jupiter during the impacts of comet Shoemaker–Levy 9. *Science* **276,** 1302–1307.

de Pater, I. 1991. The significance of microwave observations for the planets. *Phys. Rep.* **200,** 1–50.

Douglas, A. E., and I. Zanon 1964. The 2100 Å bands of CS_2. *Can. J. Phys.* **42,** 627–631.

Fegley, B. Jr., and K. Lodders 1994. Chemical models of the deep atmospheres of Jupiter and Saturn. *Icarus* **110,** 117–154.

Ford, A., and L. Browne 1973. H_2 Rayleigh and Raman scattering cross sections, *Atomic Data* **13,** 1.

Goody, R. M., and Y. L. Yung 1989. *Atmospheric Radiation: Theoretical Basis.* Oxford Univ. Press, New York.

Hammel, H. B., R. F. Beebe, A. P. Ingersoll, G. S. Orton, J. R. Mills, A. A. Simon, P. Chodas, J. T. Clarke, E. De Jong, T. E. Dowling, J. Harrington, L. F. Huber, E. Karoschka, C. M. Santori, A. Toigo, D. Yoemans, and R. A. West 1995. Hubble Space Telescope imaging of Jupiter: Atmospheric phenomena created by the impact of comet Shoemaker–Levy 9. *Science* **267,** 1288–1296.

Hansen, J. E., and L. D. Travis 1974. Light scattering in planetary atmospheres. *Space Sci. Rev.* **16,** 527–610.

Hemley, R. J., D. G. Leopold, J. L. Roebber, and V. Vaida 1983. The direct ultraviolet absorption spectrum of the $^1\Sigma_g^+ - {}^1B_2(^1\Sigma_u^+)$ transition of jet-cooled CS_2. *J. Chem. Phys.* **79,** 5219–5227.

Larson, H. P., D. S. Davis, R. Hofmann, and G. L. Bjoraker 1984. The jovian atmospheric window at 2.7 μm: A search for H_2S. *Icarus* **60,** 621–629.

Lellouch, E., G. Paubert, R. Moreno, M. C. Festou, B. Bezard, D. Bockelee-Morvan, P. Colom, J. Crovisier, T. Encrenaz, D. Gautier, A. Marten, D. Despois, D. F. Strobel, and A. Sievers 1995. Chemical and thermal response of Jupiter to the impact of comet Shoemaker–Levy 9. *Nature,* **373,** 592–595.

Lellouch, E. 1996. Chemistry induced by the impacts: Observations, In *IAU Colloquium 156,* **373,** 592–595.

Lewis, J. S. 1969. The clouds of Jupiter and the NH_3–H_2O and NH_3–H_2S systems. *Icarus* **10,** 365–378.

Liou, K. N. 1992. *Radiation and Cloud Processes in the Atmosphere.* Oxford Univ. Press, New York.

Lunine, J. L., and D. M. Hunten 1989. Abundance of condensible species at planetary cold traps: The role of moist convection. *Planet. Space Sci.* **37,** 151–166.

MacLow, M-M., and K. Zahnle 1994. Explosion of comet Shoemaker–Levy 9 on entry into the jovian atmosphere. *Astrophys. J.* **434,** 133–136.

Maillard, J.-P., P. Drossart, B. Bezard, C. de Bergh, E. Lellouch, A. Marten, J. Caldwell, J.-C. Hilco, and S. K. Atreya 1994. Methane and carbon monoxide infrared emissions observed at the Canada–France–Hawaii Telescope during the collision of Comet SL9 with Jupiter, *Geophys. Res. Lett.* **22,** 1573–1576.

Manatt, S. L., and A. L. Lame 1994. A compilation of SO_2 absorption cross sections from 106–403 nm. *J. Quant. Spectrosc. Radiat. Transfer,* in press.

Marten A., D. Gautier, T. Owen, M. J. Griffin, H. F. Matthews, D. Bockelee-Morvan, P. Colom, J. Crovisier, E. Lellouch, D. A. Naylor, G. R. Davis, G. Orton, I. de Pater, S. Atreya, B. Han, D. B. Sanders, and D. Strobel 1995. The collision of the comet Shoemaker–Levy 9 with Jupiter: Detection and evolution of HCN in the stratosphere of the planet. *Geophys. Res. Lett.* **22,** 1589–1592.

Moses, J. I. 1995a. Post SL9 sulfur photochemistry on Jupiter. *Geophys. Res. Lett.* **22,** 1597–1600.

Moses, J. I. 1995b. Nitrogen and oxygen photochemistry following SL9. *Geophys. Res. Lett.* **22,** 1601–1604.

Noll, K. S., M. A. McGrath, L. M. Trafton, S. K. Atreya, J. J. Caldwell, H. A. Weaver, R. V. Yelle, C. Barnet, and S. Edgington 1995. Hubble Space Telescope spectroscopic observations of Jupiter after the collision of comet p/Shoemaker–Levy 9. *Science* **267,** 1307–1313.

Orton, G. S., and 57 colleagues 1995. The NASA Infrared Telescope Facility investigation of comet Shoemaker–Levy 9 and its collision with Jupiter: Preliminary results. *Science* **267,** 1277–1281.

ROOS-SEROTE, M., A. BARUCCI, J. CROVISIER, P. DROSSART, M. FULCHIGNONI, J. LECACHEUX, AND F. ROQUES 1994. Metallic emission lines during the impacts of L and Q_1 of comet P/Shoemaker–Levy 9 in Jupiter, *Geophys. Res. Lett.* **22,** 1621–1624.

SMITH, P. L., K. YOSHINO, W. H. PARKINSON, K. ITO, AND G. STARK 1991. High-resolution, VUV (147–201 nm) photoabsorption cross sections for C_2H_2 at 195 and 295 K, *J. Geophys. Res.* **96,** 17,529–17,533.

SOLEM, J. C. 1994. Density and size of comet Shoemaker–Levy 9 deduced from a tidal breakup model. *Nature* **370,** 349–351.

TOMASKO, M. G., E. KARKOSCHKA, AND S. MARTINEK 1986. Observations of the limb darkening of Jupiter at ultraviolet wavelengths and constraints on the properties and distribution of stratospheric aerosols. *Icarus* **65,** 218–243.

VAN HOOSIER, M. E., J.-D. F. BARTOE, G. E. BRUECKNER, AND D. K. PRINZ 1988. Absolute solar spectral irradiance 120–400 nm (results from the solar ultraviolet spectral irradiance monitor—SUSIM—experiment on board Spacelab 2). *Astron. Lett. Commun.* **27,** 163–168.

WAGENER, R., J. CALDWELL, T. OWEN, S.-J. KIM, T. ENCRENAZ, AND M. COMBES 1985. The jovian stratosphere in the ultraviolet. *Icarus* **63,** 222–236.

WEIDENSCHILLING, S. J., AND J. S. LEWIS 1973. Atmospheric and cloud structures of the jovian planets. *Icarus* **20,** 465–476.

WEST, R. A., D. F. STROBEL, AND M. G. TOMASKO 1986. Clouds, aerosols, and photochemistry in the jovian atmosphere. *Icarus* **65,** 161–217.

WEST, R. A., E. KARKOSCHKA, A. J. FRIEDSON, M. SEYMOUR, K. H. BAINES, AND H. B. HAMMEL 1995. Impact debris particles in Jupiter's stratosphere. *Science* **267,** 1296–1301.

WU, C. Y. R., T. S. CHIEN, G. S. LIU, D. L. JUDGE, AND J. CALDWELL 1989. Photoabsorption and direct dissociation cross section of C_2H_2 in the 1530–1930 Å region: A temperature dependent study. *J. Chem. Phys.* **91,** 272–280.

WU, C. Y. R., AND D. L. JUDGE 1981. SO_2 and CS_2 cross section data in the ultraviolet region. *Geophys. Res. Lett.* **8,** 769–771.

XU, H., AND J. A. JOENS 1993. CS_2 absorption cross-section measurements from 187 nm to 230 nm. *Geophys. Res. Lett.* **20,** 1035–1037.

YELLE, R. V., AND M. A. MCGRATH 1995. Comment on ''Abundances of ammonia and carbon disulfide in the jovian stratosphere following the impact of comet Shoemaker–Levy 9,'' by Atreya *et al., Geophys. Res. Lett.,* submitted.

ZAHNLE, K., AND M-M. MACLOW 1994. The collision of Jupiter and comet Shoemaker–Levy 9, *Icarus,* **108,** 1–17.

ZAHNLE, K., M.-M. MACLOW, K. LODDERS, AND B. F. FEGLEY, JR. 1995. Sulfur chemistry in the wake of comet Shoemaker–Levy 9. *Geophys. Res. Lett.* **22,** 1593–1596.